

# Complete Characterization of a Chaotic Optical Field Using a High-Gain Self-Amplified Free-Electron Laser\*

Yuelin Li<sup>1</sup>, Samuel Krinsky<sup>2#</sup>, John W. Lewellen<sup>1</sup>, Kwang-Je Kim<sup>1</sup>,  
Vadim Sajaev<sup>1</sup>, and Stephen V. Milton<sup>1</sup>

<sup>1</sup>Advanced Photon Source, Argonne National Laboratory, Argonne, IL 60439

<sup>2</sup>Stanford Linear Accelerator Center, Stanford, CA 94309

## Abstract

For centuries chaotic light sources were the only available objects for optical science. Study of chaotic light led to the development of such important concepts as ensemble-average coherence. However, the detailed temporal structure of the underlying optical field has never been fully characterized. We report on a complete characterization of such a field from a high-gain, self-amplified spontaneous-emission (SASE) free-electron laser (FEL). The temporal structure of the amplitude and phase are measured for a single pulse and the statistics over multiple pulses is determined.

Submitted to: Physical Review Letters

#Permanent address: Brookhaven National Laboratory, Upton, NY 11973

\*Work is supported by the U. S. Department of Energy under contracts Nos. W-31-109-ENG-38, DE-AC02-98CH10886 and DE-AC03-76SF00515.

Almost all light sources encountered in our daily lives are chaotic, including the sun, incandescent light bulbs, and neon lights. Such sources also enter the field of optical communication providing unwanted white noise. Chaotic light is composed of multiple temporal and spatial coherence regimes or modes, and its statistical properties have been investigated in a time-integrated and ensemble-averaged fashion (1). One example is the famous Hanbury-Brown and Twiss experiment, where the coherence of a mercury lamp was measured using an intensity interferometer (2). Such experiments have been carried out by careful spatial and spectral filtering of the light. However, due to the lack of a source with sufficient intensity and coherence length, the temporal structure and phase evolution of the chaotic electromagnetic field has never been fully characterized.

The development of the self-amplified spontaneous-emission free-electron laser (SASE FEL) (3,4) has opened the door for a full characterization of a chaotic optical field. Starting from the shot noise in the electron bunch (5,6), the SASE power increases exponentially as the electrons propagate down the undulator. The exponential gain results from a favorable instability build-up between the electron density modulation at the resonant wavelength and the emitted light. Longitudinally, the system behaves as a narrow-band amplifier with a broadband Poisson seed. Before saturation, the output is a Gaussian random process and the radiated field is chaotic, quasimonochromatic, polarized light (7-10), with relatively long coherence length. Transversely, the output is dominated by an intense, single spatial mode. Demonstrations of such intense SASE FELs up to saturation (11-13) have now made it possible to study the evolution of the chaotic optical field, e.g., by utilizing frequency-resolved optical gating (FROG) (14), a technique widely applied in characterizing ultrafast laser pulses. In a previous paper, this

technique was used to examine the frequency chirp of the SASE FEL output and to observe the influence of the electron bunch energy chirp (15).

In this report, we characterize the 530-nm chaotic output from the SASE FEL at the Low-Energy Undulator Test Line (LEUTL) (11) at the Advance Photon Source. The field strength and phase evolution have been measured with a resolution well below the coherence length of the radiation. Our work complements previous time-integrated studies (16-18) and provides the basis for a better understanding of the physics of SASE, which will be important for applications of future SASE x-ray FELs (19,20). The main parameters for the experiment are listed in Table I. Only the first five of the eight undulators were used. The measured gain length was 0.68 m, and the SASE output was just saturated at the end of the fifth undulator.

The evolution of the SASE FEL field was measured by guiding the output of the fifth undulator to a frequency-resolved optical gating device in the second harmonic configuration (14). In this configuration, the FROG signal is  $I_{FROG}(\omega, \tau) \propto \left| \int_{-\infty}^{\infty} E(t) E(t - \tau) \exp(-i\omega t) dt \right|^2$  from which the amplitude and the phase of the input field  $E$  can be retrieved. There is an intrinsic ambiguity in the direction of time, which can be removed by analyzing the phase evolution of the field (15).

Representative examples of both the raw and reconstructed FROG traces, along with the field intensity and phase as a function of time and wavelength, are given in Figs. 1 (a-c). As expected, the behavior of the optical field is rather unpredictable from shot to shot, and no two identical shots are measured. This can be clearly seen in the examples in Figs. 1 (a-c), where (a) is dominated by a single intensity spike with relatively simple phase evolution, and (b) and (c) are composed of multiple intensity spikes. The intensity distribution among the spikes is random,

and the phase can be characterized by a smooth evolution within each spike and abrupt drifts at the edges of the spikes. We note that the raw traces are drastically different from each other but the reconstructed ones closely reproduce each of them.

We write the radiated electric field as  $E(z, t) = A(z, t) \exp(ik_r z - i\omega_r t)$ , where  $z$  represents the location along the undulator at which the SASE is observed, and  $t$  represents the temporal position in the radiation pulse. In the case of an undulator with period  $\lambda_u = 2\pi / k_u$  and magnetic field strength parameter  $K$ , the resonant frequency is  $\omega_r = k_r c = 4\pi c \gamma^2 / [\lambda_u (1 + K^2 / 2)]$ . For a cold electron beam (zero energy spread) with a long, flat-top electron bunch profile, the SASE-radiated field before saturation can be approximated as the superposition of many electromagnetic wave packets emitted from randomly distributed, individual electrons (7-10). The slowly varying envelope can be approximated by

$$A(t, z) \equiv A_0(z) \sum_{j=1}^{N_e} \exp \left[ i\omega_r t_j - \frac{(t - t_j - z/v_g)^2}{4\sigma_t^2} \left( 1 + \frac{i}{\sqrt{3}} \right) \right], \quad (1)$$

where  $N_e$  is the total number of electrons in the bunch,  $A_0(z)$  contains the exponential growth factor,  $0 \leq t_j \leq T_b$  is the random arrival time of the  $j^{\text{th}}$  electron,  $cT_b$  is the electron bunch length, and  $v_g$  is the group velocity of each wave packet. The characteristic wave-packet width  $\sigma_t = 1/(\sqrt{3} \sigma_\omega)$ , where  $\sigma_\omega = \omega_r \sqrt{3\sqrt{3} \rho / k_u z}$  is the SASE bandwidth and  $\rho$  is the FEL parameter (7-10).

Equation (1) represents the sum of a set of random phasors and requires statistical analysis and numerical evaluation. A section from a typical simulation (21) is shown in Fig. 2. The intensity and the phase evolution closely resemble those measured in the experiment in Fig. 1. Remarkably, the superposition of many wave packets results in just a few coherent regions,

represented by the intensity spikes. In SASE, this can be viewed as the result of the communication buildup that lengthens the coherence time  $T_{coh} = \sqrt{\pi} / \sigma_\omega$  (3,4,7-10) due to the slippage between the electrons and the optical wave. In photon statistics, this is described by photon bunching in a chaotic light. The fluctuation of energy per pulse is given by  $\sigma_w / \langle W \rangle = 1 / \sqrt{M}$ , where  $M = T_b / T_{coh}$  is the number of degrees of freedom or coherent modes (1,7-10). The theoretical average temporal spacing of the intensity spikes is  $\langle \Delta t \rangle = T_{coh} / 0.711$  (10), and an estimate of the rms spike width is  $\Delta\tau \equiv T_{coh} / \sqrt{2\pi} \equiv \langle \Delta t \rangle / 3.5$  (7-10).

For each individual shot, the FROG trace gives a full description of the measured optical field. Study of the shot-to-shot variation (22) provides information on the statistics of the chaotic field. We first look at the properties of the intensity spikes. Figure 3 (a) gives the measured distribution (symbols) of the normalized rms spike width  $\zeta = \Delta\tau / \langle \Delta\tau \rangle$ , where  $\langle \Delta\tau \rangle = 52$  fs is the average value of  $\Delta\tau$ , the rms spike width. The distribution peaks at a value slightly smaller than the average. It has a long tail extending to larger spike width and an abrupt drop at smaller spike width. The distribution for the spacing between the intensity maxima ( $\Delta t$ ) has also been measured and is shown in Fig. 3 (b) (symbols) as a function of  $\zeta = \Delta t / \langle \Delta t \rangle$ . The peak of the histogram is at  $\zeta = 3.3$ , and its average is at 3.5, in close agreement with theoretical expectation for a totally chaotic optical field mentioned above. In Fig. 3, we also show the comparison between the results of experiment and a numerical simulation (dashed lines) performed using the simple model of Eq. (1) (21). In Fig. 3 (a), we also present the result of an analytic calculation (solid line) by applying the analysis of random noise developed by Rice (23) to Eq. (1), which gives the distribution of the spike width normalized to its average as

$$\frac{dp(\xi)}{d\xi} = \frac{a\eta}{(a\xi)^5} \int_0^\infty \frac{d\nu}{[3 - 2/(a\xi)^2 + (1/(a\xi)^2 + \nu^2)^2]^{5/2}}, \quad (2)$$

where  $\xi = \Delta\tau/\langle\Delta\tau\rangle$ ,  $a \approx 0.8685$ , and  $\eta \approx 9.510$ . This distribution is normalized and its average value is unity. Note that for the analytical theory, the rms width of an intensity spike has been approximated by  $\sqrt{-I/I''}$ , where the intensity  $I$  and its second time-derivative  $I''$  are evaluated at the intensity maximum. For the experimental data and simulation, the rms width is estimated by measuring the full-width at half-maximum (FWHM) of those spikes with measurable FWHM and dividing by 2.35. In all cases, the spikes are assumed to have a Gaussian shape.

Since an individual intensity spike corresponds to a coherent region, the phase within the spike is correlated. On the other hand, due to the lack of communication between different coherence regions, there can be a phase jump in the transition region between two spikes. This can be seen qualitatively in Figs. 1 and 2, and is quantified by measuring the time derivative of the phase ( $\phi'$ ) of the slowly varying envelope at the intensity maxima and minima. The distribution of the measurements (symbols) presented in Figs. 4 (a) and (b) show that indeed the phase drift rate is small at the intensity maxima but may be much larger at the intensity minima. Also in Fig. 4 are the results of simulation (dashed lines) and analytic theory (solid lines), which are seen to be in good agreement with the experimental results. The theoretical calculation is again based on the analysis of random noise developed by Rice (23). It yields

$$\frac{dp_{\pm}(\nu)}{d\nu} = \frac{\chi}{\sqrt{3+\nu^4} [\sqrt{3+\nu^4} \pm (\nu^2 - 1)]^2}, \quad (3)$$

where  $\nu = \phi'/\sigma_\omega$ ,  $\chi \approx 0.7925$  is a normalizing factor, and the + and - signs mark the distributions at the intensity maxima and minima, respectively.

It is worth noting that although the simulation and theoretical work are for a long, flat bunch while the experiment data are for a relatively short bunch (in comparison with the coherence length), there is an overall good agreement between them. However, in our theoretical and numerical analysis of the distribution of the second derivative of the phase (frequency chirp) at intensity maxima (not shown in detail in this report), we do observe a difference between the long bunch and short bunch cases: while in the long bunch case the distribution is symmetric around zero, the distribution is shifted toward a positive value, as expected from Eq. (1), for the short bunches. This intrinsic positive chirp was measured in a previous paper for short bunches (15).

In previous work (17), it has been established that the SASE pulse energy is described by the gamma distribution (1,7-10,23). This type of measurement is an example of the conventional photon counting statistics. In this report, Figs. 1, 3, and 4 present a new class of experimental data on the temporal behavior of the chaotic optical field that underlies the SASE FEL output and is the first such complete characterization of the dynamic properties of a chaotic light source. Our measurements were made possible by the high intensity and relatively long coherence length of the SASE FEL and they provide information important for time-resolved experiments with future X-ray FELs, which may involve manipulating the temporal structure of the pulses (24).

The authors thank Z. Huang for helpful discussions. This work is supported by the U. S. Department of Energy under contracts Nos. W-31-109-ENG-38, DE-AC02-98CH10886 and DE-AC03-76SF00515.

## References

1. J. W. Goodman, *Statistical Optics* (John Wiley & Sons, New York, 1985).
2. R. Hanbury Brown and R. Q. Twiss, *Nature* **177**, 27 (1956).
3. A. M. Kondratenko, E. L. Saldin, *Sov. Phys. Dokl.* **24** (12), 986 (1979).
4. R. Bonifacio, C. Pellegrini, L. M. Narducci, *Opt. Commun.* **50**, 373 (1984).
5. M. C. Teich, T. Tanabe, T. C. Marshall, and J. Galayda, *Phys. Rev. Lett.* **65**, 3393 (1990).
6. P. Catravas et al., *Phys. Rev. Lett.* **82**, 5261 (1999).
7. R. Bonifacio et al., *Phys. Rev. Lett.* **73**, 70 (1994).
8. K.-J. Kim, “Towards X-ray free electron lasers,” ed. R. Bonifacio and W. A. Barletta (American Institute of Physics, New York), p. 3 (1997).
9. E. L. Saldin, E. A. Schneidmiller, M. V. Yurkov, *Nucl. Instrum. Methods Phys. Res. A* **407**, 291 (1998).
10. S. Krinsky and R.L. Gluckstern, *Phys. Rev. ST-AB* **6**, 050701 (2003).
11. S. V. Milton et al., *Science* **292**, 1953 (2001).
12. V. Ayvazyan et al., *Phys. Rev. Lett.* **88**, 104802 (2002).
13. A. Tremaine et al., *Phys. Rev. Lett.* **88**, 204801 (2002).
14. R. Trebino et al., *Rev. Sci. Instrum.* **68**, 3277 (1997).
15. Y. Li et al., *Phys. Rev. Lett.* **89**, 234801 (2002).
16. M. Hogan et al., *Phys. Rev. Lett.* **80**, 289 (1998).
17. M.V. Yurkov, *Nucl. Instrum. Methods Phys. Res. A* **483**, 51 (2002).
18. V. Sajaev et al., *Nucl. Instrum. Methods Phys. Res. A* **506**, 304 (2003).

19. SLAC Report SLAC-R-521 (Stanford Linear Accelerator Center, Stanford, CA), revised 1998.
20. DESY Report DESY97-048 (Deutsches Elektronen-Synchrotron, Hamburg), 1997.
21. In the simulation, the field is represented by Eq. (1), with  $N_e = 1600$  electrons, in a flat-top bunch of duration  $T_b = 10$  ps, with wave-packet width  $\sigma_t = 57$  fs. One hundred simulations were run, and a total of about 3600 spikes were analyzed.
22. Analysis shows that the shot-to-shot fluctuations that we study are dominated by intrinsic shot-noise effects and not by fluctuations in the average electron beam parameters.
23. S.O. Rice, Bell System Technical Journal **24**, 46 (1945). See Section 3.8.
24. C. Pellegrini, Nucl. Instrum. Methods Phys. Res. A **445**, 124 (2000).

**Table I.** Main experimental parameters

Peak current	850 A
Effective FWHM bunch length ( $T_b$ )	1.2 ps
rms normalized emittance	$9 \pi \text{ mm mrad}$
Undulator period ( $\lambda_u$ )	3.3 cm
Undulator length (each)	2.4 m
Undulator strength parameter ( $K$ )	3.1
Beam energy ( $\gamma mc^2$ )	217 MeV
Nominal radiation wavelength ( $\lambda$ )	530 nm
FWHM SASE bandwidth ( $\Delta\lambda$ )	~3 nm
Gain length ( $L_G$ )	0.68 m

## Figure captions

**Fig. 1 (a-c)** Examples of the raw and the reconstructed FROG traces, along with the field intensity and phase as a function of time and wavelength. Red: Intensity; Blue: Phase.

**Fig. 2** Field intensity (solid) and phase (dashed) as a function of time from a simulation with an electron bunch that is long compared to the coherence length using Eq. (1).

**Fig. 3** Distribution of (a) the spike width  $\Delta\tau$  and (b) the peak-to-peak spacing  $\Delta t$  between the intensity spikes normalized to the average spike width  $\langle\Delta\tau\rangle$ . Experimental data (symbols), theoretical calculation (solid line) and simulation results (dashed lines) are all presented when possible.

**Fig. 4** Distribution of phase derivative at the intensity maxima (a) and minima (b) normalized to the rms SASE FEL bandwidth. Experimental data (symbols), theoretical calculation (solid lines), and simulation results (dashed lines) are all presented. Note the different horizontal scales for (a) and the (b).

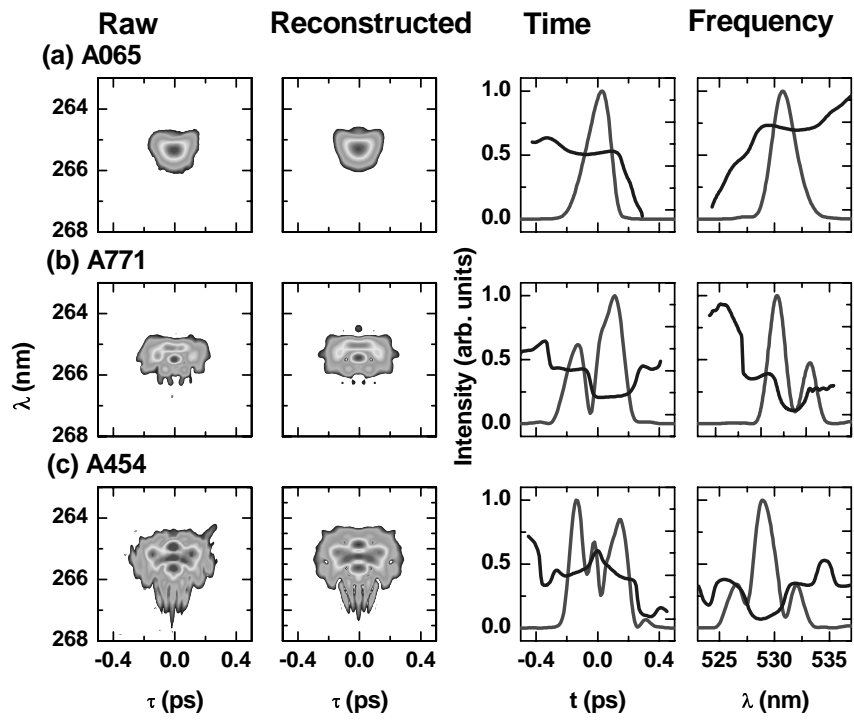


**Fig. 1 (a-c)** Examples of the raw and the reconstructed FROG traces, along with the field intensity and phase as a function of time and wavelength. Red: Intensity; Blue: Phase.

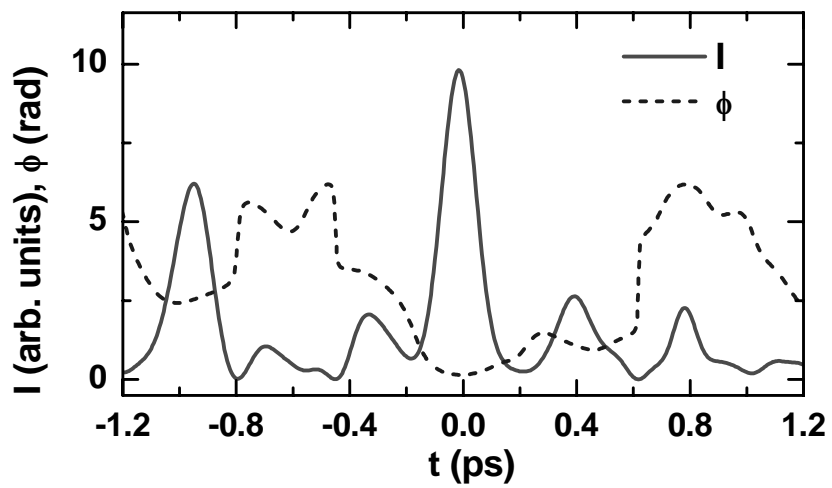


**Fig. 2** Field intensity (solid) and phase (dashed) as a function of time from a simulation with an electron bunch that is long compared to the coherence length using Eq. (1).

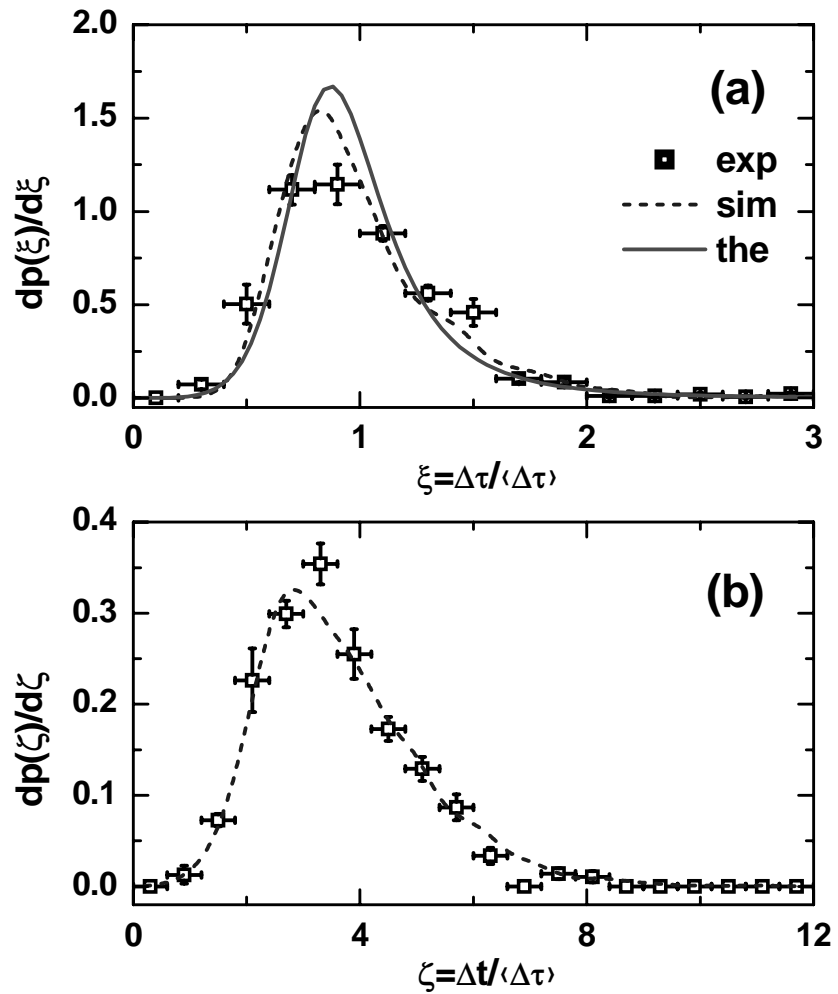


**Fig. 3** Distribution of (a) the spike width  $\Delta\tau$  and (b) the peak-to-peak spacing  $\Delta t$  between the intensity spikes normalized to the average spike width  $\langle\Delta\tau\rangle$ . Experimental data (symbols), theoretical calculation (solid line) and simulation results (dashed lines) are all presented when possible.

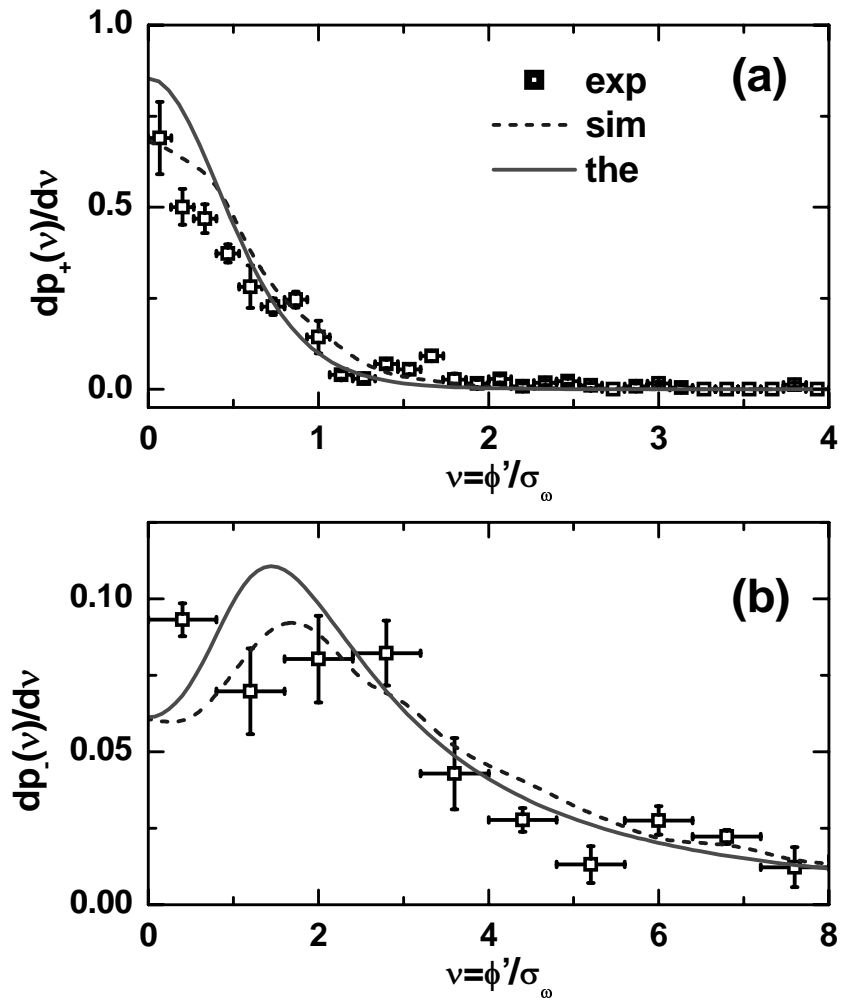


**Fig. 4** Distribution of phase derivative at the intensity maxima (a) and minima (b) normalized to the rms SASE FEL bandwidth. Experimental data (symbols), theoretical calculation (solid lines), and simulation results (dashed lines) are all presented. Note the different horizontal scales for (a) and the (b).